J Biomol NMR (2009) 45:255–264
DOI 10.1007/s10858-009-9359-2

ARTICLE

Approaches for the measurement of solvent exposure in proteins by ^{19}F NMR

Julianne L. Kitevski-LeBlanc · Ferenc Evanics · R. Scott Prosser

Received: 29 May 2009 / Accepted: 14 July 2009 / Published online: 5 August 2009

Abstract Fluorine NMR is a useful tool to probe protein folding, conformation and local topology owing to the sensitivity of the chemical shift to the local electrostatic environment. As an example we make use of ^{19}F NMR and 3-fluorotyrosine to evaluate the conformation and topology of the tyrosine residues (Tyr-99 and Tyr-138) within the EF-hand motif of the C-terminal domain of calmodulin (CaM) in both the calcium-loaded and calcium-free states. We critically compare approaches to assess topology and solvent exposure via solvent isotope shifts, ^{19}F spin–lattice relaxation rates, ^{1}H–^{19}F nuclear Overhauser effects, and paramagnetic shifts and relaxation rates from dissolved oxygen. Both the solvent isotope shifts and paramagnetic shifts from dissolved oxygen sensitively reflect solvent exposed surface areas.

Keywords ^{19}F NMR · Calmodulin · 3-Fluorotyrosine · Oxygen · Solvent exposure

Abbreviations

1D	One-dimensional
CaM	Calmodulin
CSA	Chemical shift anisotropy
DNase	Deoxyribonuclease
RNase	Ribonuclease
ID	Inner diameter
IPTG	Isopropyl β-D-1-thiogalactopyranoside
EDTA	Ethylenediaminetetraacetic acid
NMR	Nuclear magnetic resonance
OD	Outer diameter

J. L. Kitevski-LeBlanc · F. Evanics · R. S. Prosser
Department of Chemistry, University of Toronto, UTM, 3359 Mississauga Rd, North Mississauga, ON L5L 1C6, Canada

R. S. Prosser (✉)
Department of Biochemistry, University of Toronto, Toronto, ON M5S 1A8, Canada
e-mail: scott.prosser@utoronto.ca

Introduction

The fluorine nucleus is an exquisite NMR probe with which to study internal motions, ligand binding, enzymatic action, and folding in proteins (Danielson and Falke 1996; Gakh et al. 2000; Gerig 1994). The utility of the ^{19}F chemical shift in protein structure and dynamics studies arises from the paramagnetic component of the chemical shielding term associated with the fluorine lone pair electrons, which is sensitive to local van der Waals packing and electrostatic fields (Chambers et al. 1994; Feeney et al. 1996; Kubasik et al. 2006; Li and Frieden 2005; Lian et al. 1994). Examples abound in ^{19}F NMR studies of folded proteins, where a biosynthetically incorporated amino acid probe exhibits a chemical shift dispersion of 5–20 ppm (Lian et al. 1994). In this context, it may not be surprising that even the substitution of H_2O for D_2O is known to elicit an isotope shift of as much as 0.25 ppm, depending on the extent of solvent exposure of the nuclear spin probe (Gerig 1994). ^{19}F spin–lattice relaxation rates (R_1) and ^{1}H–^{19}F cross relaxation rates are known to be sensitive to environment and solvent exposure, as are corresponding paramagnetic rates arising from the dissolution of paramagnetic additives (Prosser et al. 2000). In this paper, we compare the utility of these effects—solvent isotope shifts, ^{19}F spin–lattice relaxation rates (R_1), ^{1}H–^{19}F NOEs, and paramagnetic shifts and rates from dissolved O_2—for purposes of best discriminating protein topology by ^{19}F NMR. We do this through a ^{19}F NMR study of a well-known calcium

binding protein, calmodulin (CaM), whose two tyrosine residues, located in the C-terminal domain, have been biosynthetically labeled with 3-fluorotyrosine.

Calmodulin is a ubiquitous modulator of many calcium-dependent processes in cells and it exhibits well defined conformations and binding states depending on intracellular calcium levels and the presence of a host of known binding proteins, hormones, and peptides (Crivici and Ikura 1995; Hoeflich and Ikura 2002). CaM is a well-structured, acidic protein consisting of 148 residues and possessing two structurally similar domains connected by a flexible tether (Crivici and Ikura 1995), as shown in Fig. 1. Within each domain there are two calcium binding EF-hand motifs coordinating a total of four calcium ions per protein. The well-known EF-hand motif is composed of two helices (E and F), connected by a loop of typically 12 residues, which coordinate a calcium ion with pentagonal bipyramidal symmetry (Malmendal et al. 1999). The seven ligands are provided by five sidechain carboxylate oxygens, one backbone carbonyl oxygen, and one water oxygen atom (Strynadka and James 1989). The two tyrosine residues in calmodulin are both located in the C-terminal domain where they serve distinct roles related to structure and activation. Tyr-99 is involved in calcium coordination through its main chain carbonyl atom in the first EF hand of the C-terminal domain and contributes to a small beta-strand which keeps the loops of consecutive EF hands connected (Malmendal et al. 1999). Tyr-138 does not contribute to the coordination of calcium, but is the last residue of a small beta strand in the second EF hand of the C-terminal domain. Overall, the structure of CaM is dominated by helical secondary structural elements, which are virtually identical between the calcium-loaded and calcium-free forms of the protein, where the major difference is related to helical packing (Zhang et al. 1995). In the calcium-free state the two helices of each EF hand are nearly antiparallel. Upon binding of calcium an opening of the two helices is induced resulting in an almost perpendicular arrangement with interhelical angles ranging from 86° to 101° (Babu et al. 1988). It is therefore likely that this structural reorganization will be accompanied by significant changes in sidechain conformations, specifically those involved in calcium coordination and within the helical segments themselves.

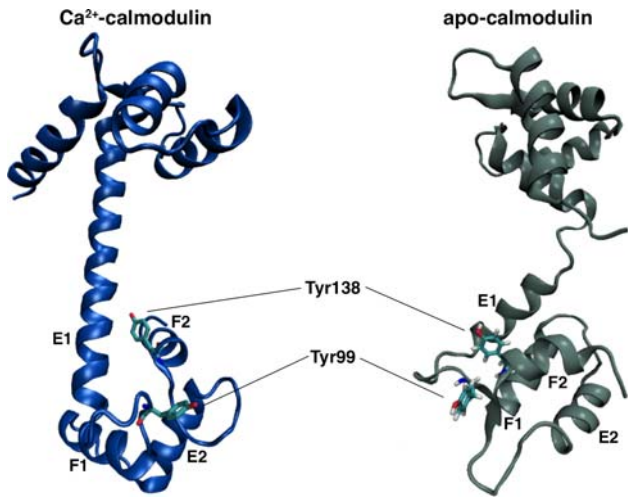

Fig. 1 Ribbon diagrams of human calmodulin in both the calcium-loaded and calcium-free states (PDB files 1CLL and 1DMO, respectively) with the location of tyrosine residues indicated. Helices associated with the EF calcium binding motifs are indicated as E1 and F1 for EF hand 1 and E2 and F2 for EF hand 2. Note that although the central helix appears rigid in the calcium-loaded X-ray structure, it has been shown by solution NMR that both calcium-loaded (Barbato et al. 1992) and calcium-free calmodulin (Tjandra et al. 1995) exhibit high flexibility in this region. The major difference between the two structures is the helical arrangement

Based on the available structures of calmodulin the solvent accessible surface area of Tyr-99 and Tyr-138 calculated using MOLMOL are 45 and 54% in calcium-loaded CaM (PDB entry 1CLL) and 36 and 47% in calcium-free CaM (PDB entry 1DMO), respectively. Here we will show that although subtle, the differences between the residues, and between the two functional forms of the protein itself, can be delineated using the aforementioned ^{19}F NMR techniques. We begin with a discussion of the biosynthetic labeling and assignment protocol as well as procedures used to assess possible perturbations arising from the use of fluorine as a probe as this is a prerequisite to any ^{19}F NMR study.

Results and discussion

Labeling and expression

Mono-, di-, and tri-fluorinated amino acid analogues can be incorporated into proteins by heterologous expression techniques, often using auxotrophic strains or induced auxotrophy (Salopek-Sondi et al. 2003). Typically, fluorine labels are minimally perturbing to the overall protein structure (Li and Frieden 2007; Xiao et al. 1998), or can be made so by fractional labeling (Feeney et al. 1996). To date, fluorinated methionine (Salopek-Sondi et al. 2003; Vaughan et al. 1999), leucine (Feeney et al. 1996), isoleucine (Mock et al. 2006), histidine (Eichler et al. 2005), phenylalanine (Li and Frieden 2005), tryptophan (Anderluh et al. 2005), and tyrosine (Hull and Sykes 1976; Sykes et al. 1974), have been incorporated into proteins via microbial expression. In our particular expression and biosynthetic labeling protocol, glyphosate, an inhibitor of aromatic amino acid synthesis, is added 1 h prior to induction of protein expression to deplete endogenous sources of

phenylalanine, tyrosine and tryptophan. At this time non-fluorinated phenylalanine and tryptophan are also added. At induction, 3-fluorotyrosine (either a ^{13}C, ^{15}N-enriched form or exactly as obtained from the commercial supplier) is added as well as IPTG to initiate protein expression at 37°C in M9 minimal media supplemented with additional nutrients and $^{15}NH_4Cl$ for uniform ^{15}N-enrichment. CaM was thus expressed uniformly labeled with 3-fluoro-L-tyrosine, and purified as described in the Materials and Methods section. ^{13}C and ^{15}N enrichment of 3-fluoro-L-tyrosine was necessary for purposes of ^{19}F NMR resonance assignments. This label was prepared using a synthetic protocol involving electrophilic fluorination of ^{13}C, ^{15}N-L-tyrosine with Selectfluor^{TM} as described in detail elsewhere (Kitevski-LeBlanc et al. 2009).

To assess the extent to which fluorotyrosine incorporation affects the backbone conformation of the protein, [^{15}N,^{1}H] HSQC spectra were acquired for fluorinated and non-fluorinated CaM under both calcium-loaded and calcium-free conditions, as shown in Fig. 2. The careful preparation of calcium-free buffers and CaM is described in the Materials and Methods section. The high degree of overlap in these spectra indicate that the global protein fold is the same in the presence and absence of 3-fluorotyrosine. The [^{15}N,^{1}H] HSQC spectra also provide qualitative evidence for native-like calcium binding affinity in the fluorinated proteins. As shown in Fig. 2, distinctive spectral features of non-fluorinated calcium-loaded and calcium-free spectra are maintained in the fluorine labeled proteins under identical sample buffer conditions. A more quantitative description of calcium binding properties is provided by measurement of the macroscopic binding constants in both the presence and absence of the fluorinated probe. This was achieved using a competitive calcium chelator assay (Linse et al. 1991) and data were fit using Caligator software (Andre and Linse 2002). The four macroscopic binding constants in the absence and presence of 3-fluorotyrosine were $K_1 = 2.4 \times 10^5\ M^{-1}$, $K_2 = 1.1 \times 10^6\ M^{-1}$, $K_3 = 3.8 \times 10^4\ M^{-1}$, $K_4 = 1.2 \times 10^5\ M^{-1}$, and $K_1 = 1.5 \times 10^5\ M^{-1}$, $K_2 = 3.1 \times 10^6\ M^{-1}$, $K_3 = 7.8 \times 10^4\ M^{-1}$, $K_4 = 8.2 \times 10^4\ M^{-1}$, respectively. In both the labeled and un-labeled protein the macroscopic binding constants indicate two cooperative binding events, previously shown to be associated with calcium binding within each domain (Linse et al. 1991), where one such event occurs at calcium concentrations approximately an order of magnitude lower than the other. Although the values obtained are comparable to those previously published under similar buffer conditions (Linse et al. 1991), it is clear that the fluorine labels do affect binding as two of the constants measured, K_3 and K_4, are affected to a greater extent and likely correspond to the domain which contains our fluorine probes. It is clear that under the current calcium-loaded buffer conditions we can be confident that the protein is fully calcium bound.

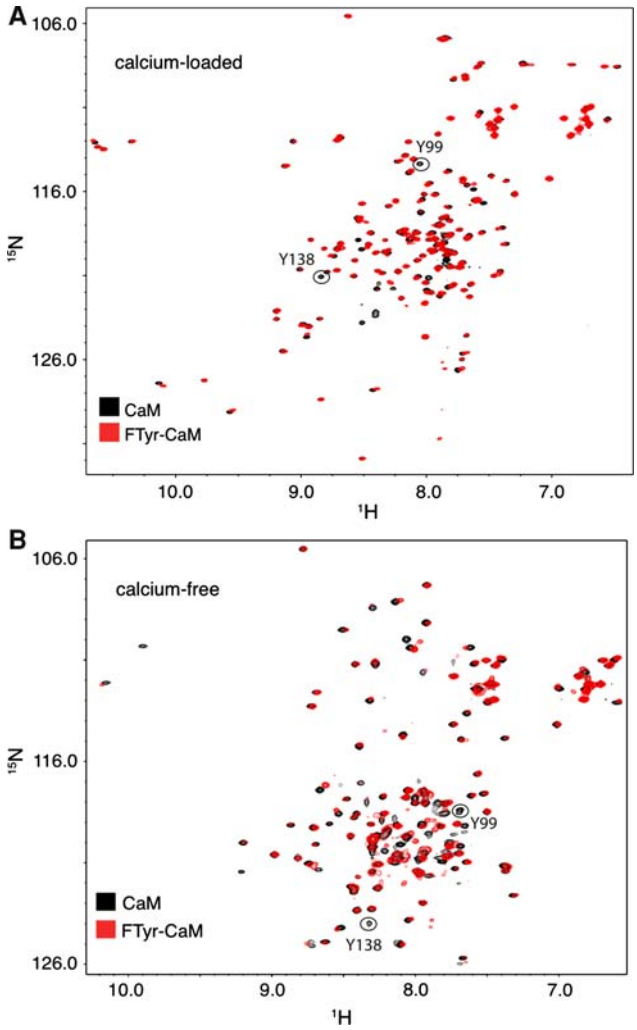

Fig. 2 [^{15}N,^{1}H] HSQC NMR spectrum of ^{15}N-enriched CaM overlaid with an equivalent spectrum of ^{15}N-enriched CaM in which Tyr99, and Tyr138 have been replaced with ^{15}N,^{13}C-enriched 3-fluorotyrosine for both calcium-loaded (**a**) and calcium-free (**b**) states at 37°C. Note that in the calcium-free state the 3-fluortyrosine was not ^{15}N-enriched, and a cross peak is thus not observed in the spectrum

Topology through chemical shift measurements

^{19}F NMR chemical shifts of fluoroaromatics are highly sensitive reporters of the electrostatic environment and tend to exhibit a broad chemical shift dispersion in proteins (Evanics et al. 2007). Downfield shifts and faster spin–lattice relaxation rates (R_1) are generally associated with more buried fluorine nuclei (Sykes et al. 1974). ^{19}F NMR spectra of the fluorinated protein in both the calcium-loaded and calcium-free states are shown in Fig. 3. Note that the peak assignments in the calcium-loaded state were obtained by a series of NMR experiments, which first

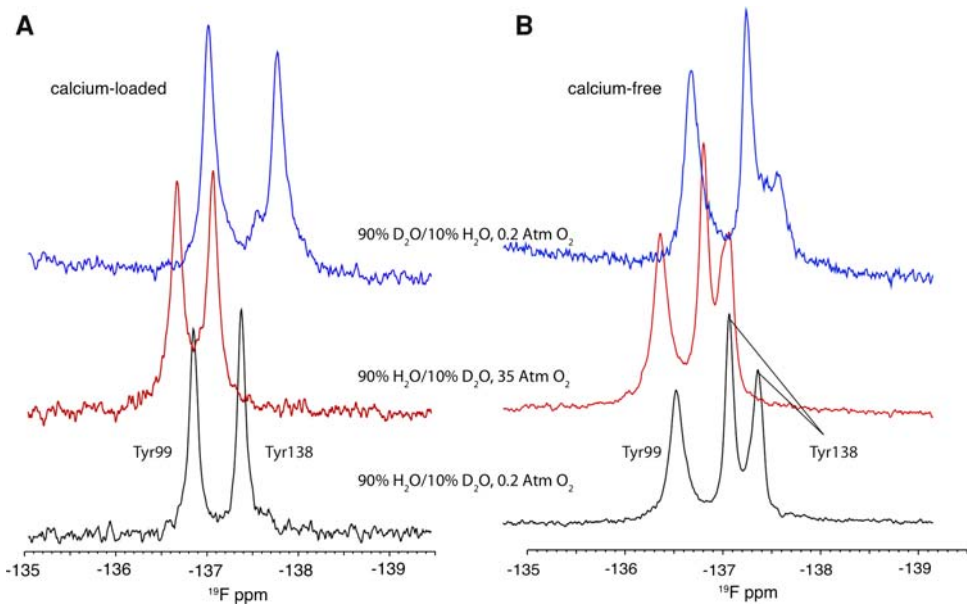

Fig. 3 ^{19}F NMR spectra of 3-fluorotyrosine labeled calcium-loaded (**a**) and calcium-free (**b**) CaM at 37°C with assignments indicated. Note that the calcium-bound CaM sample was enriched with ^{13}C,^{15}N 3-fluorotyrosine, therefore the spectra in (**a**) were obtained with ^{13}C decoupling

correlated the residue-specific ^{19}F NMR chemical shifts to the intra-residue Cδ and Hδ shifts via a CT-HCCF-COSY. Connection to the known backbone shifts was then made through the (Hβ)Cβ(CγCδ)Hδ, and HNCACB experiments as described in detail elsewhere (Kitevski-LeBlanc et al. 2009). Resonance assignments of calcium-free CaM were then obtained by monitoring the ^{19}F NMR shifts as $CaCl_2$ was titrated. The resonances arising from the two fluorotyrosine residues in calcium-loaded CaM, and calcium-free CaM are clearly resolved, indicating distinct environments, while the more downfield shifts associated with Tyr-99 are suggestive of a more buried environment. Tyr-138 is associated with two peaks in the calcium-free state, a major peak (Tyr-138M) and a minor peak (Tyr-138m), which is slightly upfield suggesting the minor peak to be the more solvent exposed of the two. Interestingly, the chemical shift of Tyr-138m is coincident with the chemical shift of this residue in the calcium-loaded form. We therefore propose that this minor peak may represent a calcium-bound like conformation with respect to Tyr-138, where the chemical shift difference implies that exchange between the so called major and minor conformers is slower than $\sim$5 ms. It is also apparent that the total integrated area of Tyr-138 is greater than that of Tyr-99. ^{19}F CPMG experiments (data not shown) indicate that Tyr-99 is undergoing chemical exchange, and it is possible that the missing peak intensity is associated with an unobservable exchange broadened state.

The ^{19}F spin–lattice relaxation rates, R_1, corroborate the above chemical shift trends; faster relaxation rates, observed for Tyr-99, indicate greater burial, as summarized in Table 1. Curiously the relaxation rate for Tyr-138m is the highest at all temperatures, indicating that although this resonance is the most upfield, it appears to be in greater dipolar contact with the protein interior relative to the other residues. It should be noted that although spin-1/2 relaxation is in general dominated by a dipole–dipole mechanism, the large chemical shift anisotropy (CSA) associated with the fluorine nucleus compounded by modern magnetic field strengths is expected to result in significant weakening of the correlation between dipolar contact, or burial, and the ^{19}F relaxation rate.

While the chemical shifts and R_1 measurements report on the degree of burial, one can directly assess solvent exposure using solvent induced isotope shifts. The exchange of 90% H_2O with 90% D_2O can shift solvent

Table 1 Chemical shifts and spin–lattice relaxation rates for ^{19}F nuclei in 3-fluorotyosine labeled calcium-loaded and calcium-free calmodulin

	δ (ppm)	R_1 (Hz) 5°C	R_1 (Hz) 15°C	R_1 (Hz) 25°C
Ca^{2+}-loaded				
Tyr-99	−136.98	1.10 ± 0.06	1.34 ± 0.05	1.60 ± 0.05
Tyr-138	−137.48	0.96 ± 0.05	0.90 ± 0.07	1.01 ± 0.04
Ca^{2+}-free				
Tyr-99	−136.61	1.57 ± 0.05	1.57 ± 0.06	1.69 ± 0.04
Tyr-138M	−137.07	1.24 ± 0.04	1.24 ± 0.04	1.35 ± 0.03
Tyr-138m	−137.39	2.03 ± 0.48	2.17 ± 0.43	2.29 ± 0.55

Table 2 Paramagnetic rates, and shifts and solvent isotope shifts for calcium-loaded and calcium-free calmodulin

	R_1 (Hz) O_2 35 Atm	ΔR_1 (Hz)	$\Delta\delta$ O_2 (ppm)	$\Delta\delta$ * O_2 (ppm)	$\Delta\delta$ D_2O–H_2O (ppm)	$\Delta\delta$ * D_2O–H_2O (ppm)	$\Delta\delta$ * $O_2/\Delta\delta$ * D_2O–H_2O
Ca^{2+}-loaded							
Tyr-99	8.13 ± 0.21	7.03 ± 0.22	0.180	0.623	−0.113	0.456	1.697
Tyr-138	10.0 ± 0.17	9.04 ± 0.17	0.300	1.038	−0.302	1.218	1.058
Ca^{2+}-free							
Tyr-99	8.50 ± 0.12	6.72 ± 0.13	0.130	0.450	−0.075	0.429	1.050
Tyr-138M	9.24 ± 0.15	7.92 ± 0.15	0.216	0.747	−0.178	1.017	0.735
Tyr-138m	9.70 ± 0.15	7.84 ± 0.57	0.260	0.900	−0.182	1.04	0.865

Parameters marked with an asterisk were normalized to free 6-fluortryptophan in buffer solution. All measurements were made at 25°C

accessible resonances by as much as 0.25 ppm (Gerig 1994). The solvent isotope shifted ^{19}F NMR spectra for calcium-loaded and calcium-free CaM are shown in Fig. 3, and the solvent induced isotope shifts are summarized in Table 2. Note that the most pronounced solvent isotope shifts are observed for Tyr-138 corroborating the above finding based on diamagnetic shifts and R_1 data, that it exhibits the greatest solvent exposure. In contrast to the R_1 value obtained for Tyr-138m, the solvent isotope shift associated with this resonance indicates a high degree of solvent exposure of the minor conformer.

Topology through paramagnetic additives

Solvent exposure and conversely, burial, can also be substantiated by the measurement of shifts or relaxation rate enhancement from dissolved paramagnetic additives. For example, the addition of minute quantities of 4-hydroxy-2,2,6,6-tetramethylpiperidine-N-oxyl (TEMPOL) exerts prominent changes in spin–spin or spin–lattice relaxation rates on solvent accessible spins (Niccolai et al. 2003). Alternatively, a variety of chelated paramagnetic metal species may be used to probe topology and solvent exposure through local relaxation rate enhancements. O_2 is also a convenient paramagnetic additive, particularly in conjunction with ^{19}F NMR studies, since both shifts and relaxation rate enhancements are readily observed at oxygen partial pressures of 20–50 bar (Evanics et al. 2007). Paramagnetic spin–lattice relaxation rates (obtained by simply measuring the difference between R_1 in the presence of dissolved O_2 and under atmospheric conditions) and paramagnetic shift data are summarized in Table 2 for each of the fluorinated residues. While paramagnetic rate enhancements at 25°C turn out to be modestly greater for Tyr-138 in the calcium-loaded form (i.e., 9.04 vs. 7.03 s^{-1} for Tyr-138 and Tyr-99, respectively) the paramagnetic shifts are observed to be significantly higher for Tyr-138 (i.e., 0.30 vs. 0.18 ppm for Tyr-138 and Tyr-99, respectively), reaffirming the tentative conclusion based on chemical shifts and R_1 under atmospheric oxygen levels that the fluorine nucleus of Tyr-99 is on average more buried than that of Tyr-138. Under the same conditions, a similar conclusion is reached for calcium-free CaM where both Tyr-138M and Tyr-138m exhibit higher rate enhancements, and correspondingly higher paramagnetic shifts than Tyr-99. Although the observed rate enhancements for Tyr-138M and Tyr-138m are comparable, the paramagnetic shift is highest for the minor conformer suggesting it is most solvent exposed. Note that the O_2 paramagnetic shifts exhibit a wider range of effects than the paramagnetic rates. Subtle differences between paramagnetic rates and shifts in ^{19}F NMR are expected since the relaxation and shift terms are entirely different in origin, while dynamics and distance effects further complicate the analysis.

Paramagnetic effects from dissolved oxygen are not purely steric in origin. One expects more hydrophobic regions to experience a more favorable interaction with O_2 which should be reflected in heightened paramagnetic effects due to greater local partitioning (Teng et al. 2006). It has been shown that one can distinguish between the steric and local partitioning effects by separately making use of hydrophobic and hydrophilic shift reagents (Evanics et al. 2006). Two such complimentary measurements involve the solvent isotope shifts, and O_2-induced paramagnetic shifts, where O_2 serves as the hydrophobic probe and the D_2O–H_2O mixture as the hydrophilic probe. Thus, assuming that the steric factors are similar for water and oxygen, we can take the ratio of the paramagnetic shift to the isotope shift (normalized to free fluorotryptophan in the sample buffer), $\Delta\delta$ * $O_2/\Delta\delta$ * D_2O–H_2O, as a relative measure of hydrophobicity. The data, shown in Fig. 3 and summarized in Table 2, indicate that in the calcium-loaded form, Tyr-99 is situated in a more hydrophobic environment than Tyr-138, with hydrophobicity measures of 1.697 and 1.058, respectively. This is also consistent with the

results of the ^{1}H–^{19}F NOE measurements in which aliphatic ^{1}H saturation resulted greater cross-relaxation to Tyr-99. In the calcium-free state the hydrophobicity index, $\Delta\delta \times O_2/\Delta\delta \times D_2O$–$H_2O$, also suggests that Tyr-99 is situated in a more hydrophobic environment than Tyr-138M or Tyr-138m. Interestingly, although the chemical shift of the minor conformer is coincident with Tyr-138 in the calcium-loaded form, the hydrophobicity index for Tyr-138m falls very close to the average between Tyr-138M and Tyr-138. This may reflect some degree of local conformational fluctuations in Tyr-138m resulting in a hydrophobicity index value distinct from that of Tyr-138. The exchange between the major and minor conformational states of Tyr-138 in calcium-free CaM appears to be slower than the $\sim$5 ms dictated by the chemical shift difference, and is currently under further investigation.

Heteronuclear ^{1}H–^{19}F NOEs

^{1}H–^{19}F cross-relaxation rates can also be used to assess solvent accessibility or burial of specific fluorinated sites, assuming that cross-relaxation rates between ^{19}F and H_2O can be distinguished from those between ^{19}F and the protein interior. The heteronuclear NOE is well established (Rinaldi 1983) as are ^{1}H–^{19}F NOEs in proteins (Campos-Olivas et al. 2002; Cistola and Hall 1995; Yu et al. 2006). For example, the work of Campos-Olivas et al. established inter-residue ^{1}H–^{19}F connectivities from a 5-fluorotryptophan substituted protein consisting of 56-residues, while Hajduk et al. utilized intermolecular ^{1}H–^{19}F NOEs to establish protein-ligand structural restraints in complexes of the anti-apoptotic protein Bcl-xL and several fluorinated drugs (Yu et al. 2006). What becomes clear from these few examples is that the magnitude of the ^{1}H–^{19}F NOE is made significantly smaller in slow tumbling systems and at higher field strengths particularly in situations where the fluorine probe possesses a large CSA. In our hands it proved impossible to observe a prominent ^{1}H–^{19}F NOE (over 12 h) between the 3-fluorotyrosine resonances and the δ-proton resonances or indeed, a backbone ^{1}H resonance which would have simplified assignment.

The ^{1}H–^{19}F NOE is suspected to be weak in our system for two main reasons. In cases where the fluorine resonance is saturated or inverted, the magnetization can return to equilibrium via the CSA relaxation mechanism significantly reducing ^{1}H–^{19}F cross relaxation. An additional problem is the reduced efficiency of the relevant spectral density terms associated with cross relaxation in the heteronuclear case (versus the homonuclear NOE). In the absence of CSA effects the magnitude of the ^{19}F NOE effect upon saturation of a ^{1}H spin may be expressed as (Neuhaus and Williamson 2000)

$$\mathrm{NOE} = \frac{I_0 - I}{I} = \frac{\sigma_{HF}}{\rho_{HF}} = \frac{\gamma_H}{\gamma_F} \frac{6J(\omega_H + \omega_F) - J(\omega_H - \omega_F)}{J(\omega_H - \omega_F) + 3J(\omega_F) + 6J(\omega_H + \omega_F)} \quad (1)$$

where γ_F and γ_H define the gyromagnetic ratios of the ^{19}F and ^{1}H nuclei, σ_{HF} and ρ_{HF} represent the cross-relaxation and auto-relaxation terms, respectively, and $J(\omega)$ represent the familiar spectral density functions. In large proteins, the dominant spectral density terms for σ_{HF} are $J(0)$ and $J(\omega_H - \omega_F)$ for the homo- and hetero-nuclear cases, respectively. In CaM specifically, where we assume that the protein undergoes isotropic reorientation with a correlation time (τ_c) of 6.30 ns (Barbato et al. 1992), the relevant spectral densities become $J(\omega_H - \omega_F) = 4.28$ ns rad^{-1}, $J(0) = 12.60$ ns rad^{-1}, making the heteronuclear cross relaxation term 3.4 times less efficient than the homonuclear equivalent. In addition, an observable NOE is compromised by internal motions which have been shown to result in significantly reduced enhancements in 3-fluorotyrosine labeled alkaline phosphatase (Hull and Sykes 1975).

In situations where an explicit ^{1}H–^{19}F NOE cannot be observed, cross-relaxation between all aliphatic or water protons and the fluorine nucleus of interest provides a perspective on topology—i.e., is the ^{19}F nucleus in question buried in the protein or facing the water exterior? Figure 4 reveals a series of difference spectra showing a NOE effect on both Tyr-99 and Tyr-138 (Tyr-138M only) as a function of a selective presaturation on either the water (Fig. 4a, b) or the ^{1}H aliphatic region (Fig. 4c, d), for a range of mixing times as indicated. Due to the low signal intensity of Tyr-138m and the aforementioned weaknesses of the heteronuclear NOE we were unable to obtain a measurable ^{1}H–^{19}F NOE to Tyr-138m over a 12 h time span. The results from the two complementary experiments indicate that Tyr-99 appears to be in greater dipolar contact with the aliphatic protons, while Tyr-138 is in greater contact with water. This corroborates the above topology experiments (shift and T_1 measurements, isotope effects, and paramagnetic effects from dissolved O_2) all of which suggest that the two fluorotyrosine labels are in markedly different environments.

Conclusions and final remarks

In this paper, we have explored a variety of alternative approaches for the measurement of surface topology of ^{19}F-labeled sites using 3-fluorotyrosine labeled calmodulin, in both the calcium-loaded and calcium-free states as a case study. In particular, solvent isotope shifts, paramagnetic shifts and rates from dissolved O_2, and ^{1}H–^{19}F heteronuclear NOEs resulting from ^{1}H aliphatic and water

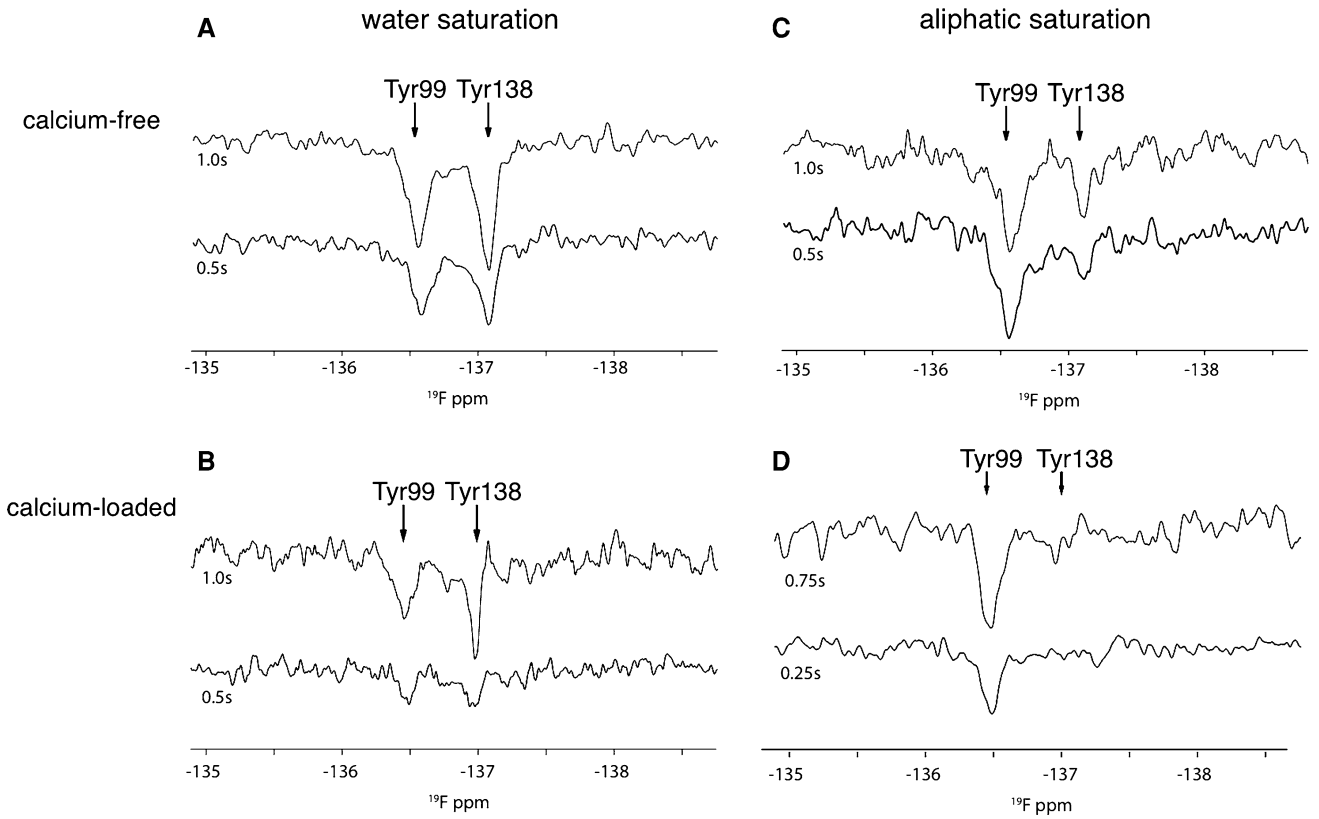

Fig. 4 ^{1}H–^{19}F 1D difference NOE initiated by saturation of either water (**a**, **b**) or aliphatic protons (**c**, **d**), for calcium-free CaM, shown in the upper two panels, and calcium-loaded CaM, shown in the lower two panels. NOE mixing times are indicated on the left margin of each spectrum. The observed enhancements for water (aliphatic) saturation and a 1 s mixing time correspond to 3.0 and 2.1% (1.7 and 2.4%) for Tyr-99 in calcium-free and calcium-loaded calmodulin, respectively. The corresponding enhancements for Tyr-138 are 2.6 and 2.8% (0.6 and 0.4%)

presaturation, all provide a consistent picture in which Tyr-99 is more buried and less solvent exposed than Tyr-138 in both the calcium-loaded and calcium-free states. In the calcium-free state, an interesting slow equilibrium between a major sidechain conformer and a minor calcium-bound like state was also consistently observed for Tyr-138 (i.e., Tyr-138M and Tyr-138m). Further characterization of this equilibrium is currently under investigation in our lab.

A tentative comparison of the relative sensitivity of the solvent isotope shifts and the paramagnetic shifts and rates from dissolved O_2 can be made by examining the correlation between the above parameters and the solvent exposed surface areas, as determined from the high resolution structures of the calcium-loaded and calcium-free states of CaM. In the case of either solvent isotope shifts or O_2-induced paramagnetic shifts, a small change ($\sim$10%) in solvent exposure is associated with a corresponding change in the measured parameter. Further, it is shown in Fig. 5 that the geometric average of the solvent

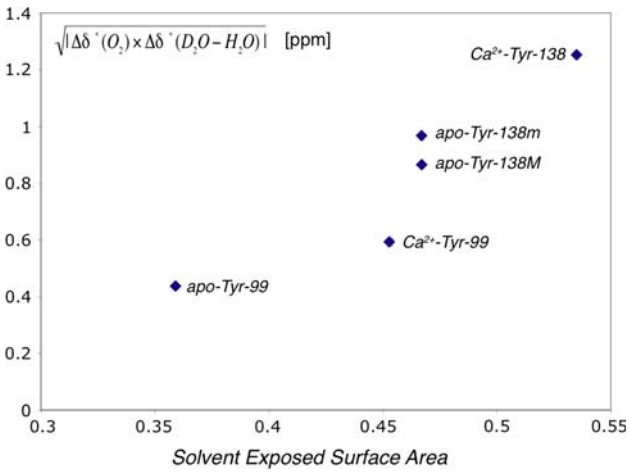

Fig. 5 Graphical representation of the correspondence between the geometric average of the experimentally determined solvent isotope shifts, $\Delta\delta$ * (D_2O–H_2O), and O_2-induced paramagnetic shifts, $\Delta\delta$ * (O_2), given by $\sqrt{|\Delta\delta * (O_2) \times \Delta\delta * (D_2O–H_2O)|}$, as a function of solvent exposed surface areas calculated from each of the two high resolution structures for CaM in the calcium-loaded ad calcium-free states

isotope shifts and paramagnetic shifts from dissolved O_2, $\sqrt{|\Delta\delta*(O_2)\times\Delta\delta*(D_2O–H_2O)|}$, correlates best with solvent exposure since partitioning effects associated with hydrophobic regions are factored out (Evanics et al. 2006).

The hydrophobicity index calculated as the normalized paramagnetic shift from dissolved O_2, divided by the normalized solvent isotope shifts also proved to be a useful tool in the analysis of protein topology. In both the calcium-loaded and calcium-free states, Tyr-99 proved to exist in a more hydrophobic environment, while the minor conformer associated with Tyr-138 in the calcium-free state (Tyr-138m) appeared to be situated in an environment that was between that of the calcium-loaded and dominant calcium-free state for this residue.

The above analysis suggests that the solvent exposure and surface topology can be reliably assessed by ^{19}F NMR, by making use of solvent isotope shifts, O_2 paramagnetic shifts, and to some extent HF cross-relaxation. It is anticipated that such measurements might nicely complement any ^{19}F NMR study of proteins, as the observed effects are not restricted to aromatic fluorine probes.

Materials and methods

Expression and purification of uniformly ^{15}N,^{13}C-L-3-fluorotyrosine labeled CaM

Incorporation of ^{15}N,^{13}C-enriched L-3-fluorotyrosine via heterologous expression (Evanics et al. 2007) as well as purification of calmodulin (Ikura et al. 1990) was performed as previously described with slight modifications. A plasmid (pET21b) encoding *Xenopus laevis* calmodulin (residues 1–148) was transfected into BL21(DE3) under the control of the *T*7 promoter. LB broth inoculated with a single colony was grown overnight and used to inoculate 1 L of M9 minimal media supplemented with 0.3% D-glucose, 0.1% $^{15}NHCl_4$, 100 mg/L ampicillin, 10 mg/L thiamine, 10 mg/L biotin, 1 mM $MgSO_4$, and 0.1 mM $CaCl_2$. Uniform labeling with fluorotyrosine was achieved by the introduction of 1 g/L glyphosate, 75 mg/L DL-tryptophan, and 75 mg/L DL-phenylalanine to shaking bacterial cultures at 37°C which had reached an OD_{600} of 0.600. Once cell cultures achieve an OD_{600} 0.800 (after approximately 1 h), 18 mg/L ^{13}C,^{15}N-L-3-fluorotyrosine was added and expression was induced with the addition of 238 mg/L IPTG. Cell cultures were harvested after 3.5 h by centrifugation at 7,000 rpm for 20 min. Cells were then resuspended in 50 mM NaH_2PO_4, 300 mM NaCl, 10 mM imidazole, 1 mM PMSF pH 8 and lysed by incubation at 4°C in the presence of 1 mg/mL lysozyme for 30 min, followed by sonication. After addition of DNase (10 μg/mL) and RNase (5 μg/mL), the suspension was centrifuged at 9,000 rpm for 20 min at 4°C and the cleared lysate was purified using Ni-NTA Agarose resin (Qiagen, Mississauga, Ontario, Canada). The labeled protein was further purified using phenyl sepharose as described previously (Ikura et al. 1990). Pooled protein samples were buffer exchanged into 20 mM BIS-Tris, 0.1 M KCl, 9 mM $CaCl_2$, 0.2% NaN_3 at pH 7.5. Calcium-free calmodulin samples were prepared as previously described (Zhang et al. 1995) with slight modification. All buffers used in the preparation of calcium-free CaM were made with water which had been decalcified using Chelex-100 resin and stored in plastic bottles which had been treated with 5 mM EDTA followed by extensive rinsing with decalcified water. Ethylenediaminetetraacetic acid (EDTA) was added to purified, dilute protein samples (~200–500 μM) to a final concentration of 20 mM, followed by precipitation with trichloroacetic acid (TCA). The sample was redissolved in 25 mM NH_4HCO_3 and passed through a Sephadex G-25 column. Collected protein was then exchanged into 20 mM Bis–Tris, 0.1 M KCl, 2 mM EDTA, 0.2% NaN_3 at pH 7.5 for NMR experiments and macroscopic binding constant determination.

Determination of macroscopic binding constants

Macroscopic calcium binding constants were measured using a competitive chelator assay as described previously (Linse et al. 1991). 5,5′-Br_2-BAPTA was obtained from Molecular Probes (Eugene, Oregon). Briefly, calmodulin and 3-fluorotyrosine labeled calmodulin were decalcified as described above and titrated with 1 mM $CaCl_2$ in the presence of 5,5′-Br_2-BAPTA in 20 mM Bis-Tris, 0.1 M KCl, pH 7.5, prepared with decalcified water at 25°C until $OD_{263\ nm}$ indicated saturation. The raw data was fit using Caligator software (Andre and Linse 2002) to obtain K_1 through K_4.

NMR experiments

NMR experiments were performed on a 600 MHz Varian Inova spectrometer (Varian Inc., Palo Alto, CA). For direct observe ^{19}F NMR experiments, and all HCN experiments, a 5 mm HCN/FCN triple resonance single gradient salt-tolerant cryogenic probe, tunable to either ^{1}H or ^{19}F, was used. All calmodulin sample concentrations were 1.5–2 mM in 90%H_2O/10%D_2O, 0.1 M KCl, 7.1 mM $CaCl_2$, 0.2% NaN_3 at pH 7.5. 1-D ^{19}F NMR spectra were obtained at 30°C with 256 transients, using a spectral width of 15,000 Hz and a π/2 pulse width of 11 μs. ^{19}F spin–lattice relaxation times (T_1) were determined using an inversion recovery sequence (i.e., 180°-τ–90°) with a total of 12 τ values ranging from 1 ms to 4.5 s, and a repetition time of

4 s. For purposes of measuring paramagnetic rates associated with spin–lattice relaxation in the presence of dissolved oxygen, T_1 experiments were repeated under an oxygen partial pressure of 35 Atm. Note that the pressures used to induce paramagnetic effects from dissolved oxygen are extremely low (20–40 Atm) relative to pressures which typically affect detectable structural perturbations (Wilton et al. 2008). We have observed minor perturbations at or above 50 Atm in membranes (Prosser et al. 2001) and disordered proteins (Bezsonova et al. 2006), however, folded proteins are typically less compressible. These experiments necessitated the use of a 5 mm OD, 3 mm ID sapphire NMR sample tube (Saint Gobain-Saphikon Crystals, Milford, NH). Samples were generally equilibrated under 50 Atm oxygen partial pressure at 5°C for 2 days, then equilibrated overnight in the magnet at the desired temperature and partial pressure. Open Swagelok connections (Swagelok, Solon, OH) to a pressurized oxygen supply were used to maintain the pressure throughout the experiment. For solvent isotope shift measurements the buffer was exchanged from 90% H_2O to 90% D_2O using centrifugation filters by repetition of diluting the sample tenfold followed by concentration 4 times. Based on the consistency of our measurements under the various conditions employed, it seems clear that no major structural perturbations result from exchange into deuterated buffer conditions. ^{19}F NMR transverse (T_2) relaxation times were measured using a Hahn echo sequence (i.e., 90°-τ–180°-τ) with 12 τ values ranging from 0.64 to 11.2 ms, and a repetition time of 2.75 s. ^{1}H–^{19}F steady-state NOE measurements were performed on a HFCN quad probe (Varian Inc., Palo Alto, CA) using a differencing FHOESY experiment (Lix et al. 1996; Rinaldi 1983). Fluorine resonances and in alternate scans either water, aliphatic or all protons (data not shown) were saturated for 12 ms, followed by a mixing period of 0, 0.5 and 1.0 s for water presaturation, and 0, 0.1, 0.25, 0.5, 0.75, 1, 1.5, and 2.0 s for aliphatic proton presaturation. Proton saturation was optimized in a separate ^{1}H direct-detect experiment and found to be optimal using an RF field of 1,838 Hz for the 12 ms saturation period. The use of simultaneous saturation of fluorine and proton resonances generated NOE difference spectra with minimal artifacts when compared to other heteronuclear NOE pulse sequences. ^{19}F spectra resulting from the difference NOE were collected using 8,192 transients, a spectral width of 2,200 Hz, and a repetition time of 3 s. [^{15}N,^{1}H] HSQC pulse sequences were obtained from Biopack software (Varian Inc.) and typically were collected in 4 scans with 96 increments spanning 2,000 Hz in the indirect dimension. All NMR data were processed using NMRPipe/NMRDraw (Delaglio et al. 1995), and analyzed with NMRView software (Johnson and Blevins 1994).

Acknowledgments We wish to thank Professor Mitsu Ikura (University of Toronto) for providing the plasmid for *Xenopus laevis* calmodulin. We would like to acknowledge Prof. Lewis Kay (University of Toronto), Ranjith Muhandiram (University of Toronto), and many members from Varian Inc. and the Varian applications group (George Gray, Eriks Kupce, Mikhail Reibarkh, Bao Nguyen, and Christine Hofstetter) for their continued help. Julianne Kitevski-LeBlanc wishes to acknowledge the Natural Sciences and Engineering Research Council of Canada (NSERC) for a doctoral fellowship and RSP acknowledges NSERC, and the Ontario government for financial support through the NSERC discovery and Provincial Research Excellence Award (PREA) programs.

References

Anderluh G, Razpotnik A, Podlesek Z, Macek P, Separovic F, Norton RS (2005) Interaction of the eukaryotic pore-forming cytolysin equinatoxin II with model membranes: F-19 NMR studies. J Mol Biol 347:27–39

Andre I, Linse S (2002) Measurement of Ca2+ -binding constants of proteins and presentation of the Caligator Software. Anal Biochem 305:195–205

Babu YS, Bugg CE, Cook WJ (1988) Structure of calmodulin refined at 2.2 a resolution. J Mol Biol 204:191–204

Barbato G, Ikura M, Kay LE, Pastor RW, Bax A (1992) Backbone dynamics of calmodulin studied by N-15 relaxation using inverse detected 2-dimensional NMR-spectroscopy—the central helix is flexible. Biochemistry 31:5269–5278

Bezsonova I, Korzhnev DM, Prosser RS, Forman-Kay JD, Kay LE (2006) Hydration and packing along the folding pathway of SH3 domains by pressure-dependent NMR. Biochemistry 45:4711–4719

Campos-Olivas R, Aziz R, Helms GL, Evans JNS, Gronenborn AM (2002) Placement of F-19 into the center of GB1: effects on structure and stability. FEBS Lett 517:55–60

Chambers SE, Lau EY, Gerig JT (1994) Origins of fluorine chemical-shifts in proteins. J Am Chem Soc 116:3603–3604

Cistola DP, Hall KB (1995) Probing internal water-molecules in proteins using 2-dimensional F-19–H-1 NMR. J Biomol NMR 5:415–419

Crivici A, Ikura M (1995) Molecular and structural basis of target recognition by calmodulin. Annu Rev Biophys Biomol Struct 24:85–116

Danielson MA, Falke JJ (1996) Use of F-19 NMR to probe protein structure and conformational changes. Annu Rev Biophys Biomol Struct 25:163–195

Delaglio F, Grzesiek S, Vuister GW, Zhu G, Pfeifer J, Bax A (1995) NMRPipe—a multidimensional spectral processing system based on UNIX pipes. J Biomol NMR 6:277–293

Eichler JF, Cramer JC, Kirk KL, Bann JG (2005) Biosynthetic incorporation of fluorohistidine into proteins in *E. coli*: a new probe of macromolecular structure. Chembiochem 6:2170–2173

Evanics F, Bezsonova I, Marsh J, Kitevski JL, Forman-Kay JD, Prosser RS (2006) Tryptophan solvent exposure in folded and unfolded states of an Sh3 domain by F-19 and H-1 NMR. Biochemistry 45:14120–14128

Evanics F, Kitevski JL, Bezsonova I, Forman-Kay J, Prosser RS (2007) F-19 NMR studies of solvent exposure and peptide binding to an SH3 domain. Biochimica Et Biophysica Acta-General Subjects 1770:221–230

Feeney J, McCormick JE, Bauer CJ, Birdsall B, Moody CM, Starkmann BA, Young DW, Francis P, Havlin RH, Arnold WD, Oldfield E (1996) F-19 nuclear magnetic resonance chemical shifts of fluorine containing aliphatic amino acids in

proteins: studies on *Lactobacillus casei* dihydrofolate reductase containing (2 s, 4 s)-5-fluoroleucine. J Am Chem Soc 118: 8700–8706

Gakh YG, Gakh AA, Gronenborn AM (2000) Fluorine as an NMR probe for structural studies of chemical and biological systems. Magn Reson Chem 38:551–558

Gerig JT (1994) Fluorine NMR of proteins. Prog Nucl Magn Reson Spectrosc 26:293–370

Hoeflich KP, Ikura M (2002) Calmodulin in action: diversity in target recognition and activation mechanisms. Cell 108:739–742

Hull WE, Sykes BD (1975) Fluorotyrosine alkaline-phosphatase—internal mobility of individual tyrosines and role of chemical-shift anisotropy as a F-19 nuclear spin relaxation mechanism in proteins. J Mol Biol 98:121–153

Hull WE, Sykes BD (1976) Fluorine-19 nuclear magnetic-resonance study of fluorotyrosine alkaline-phosphatase—influence of zinc on protein structure and a conformational change induced by phosphate binding. Biochemistry 15:1535–1546

Ikura M, Marion D, Kay LE, Shih H, Krinks M, Klee CB, Bax A (1990) Heteronuclear 3D NMR and isotopic labeling of calmodulin—towards the complete assignment of the H-1-NMR spectrum. Biochem Pharmacol 40:153–160

Johnson BA, Blevins RA (1994) NMRView—a computer-program for the visualization and analysis of NMR data. J Biomol NMR 4:603–614

Kitevski-LeBlanc JL, Al-Abdul-Wahid, Prosser RS (2009) A mutagenesis-free approach to assignment of F-19 NMR resonances in biosynthetically labeled proteins. J Am Chem Soc 131:2054

Kubasik MA, Daly E, Blom A (2006) F-19 NMR chemical shifts induced by a helical peptide. Chembiochem 7:1056–1061

Li H, Frieden C (2005) NMR studies of 4-F-19-phenylalanine-labeled intestinal fatty acid binding protein: evidence for conformational heterogeneity in the native state. Biochemistry 44:2369–2377

Li HL, Frieden C (2007) Observation of sequential steps in the folding of intestinal fatty acid binding protein using a slow folding mutant and F-19 NMR. Proc Natl Acad Sci USA 104:11993–11998

Lian CY, Le HB, Montez B, Patterson J, Harrell S, Laws D, Matsumura I, Pearson J, Oldfield E (1994) F-19 nuclear-magnetic-resonance spectroscopic study of fluorophenylalanine-labeled and fluorotryptophan-labeled avian egg-white lysozymes. Biochemistry 33:5238–5245

Linse S, Helmersson A, Forsen S (1991) Calcium-binding to calmodulin and its globular domains. J Biol Chem 266:8050–8054

Lix B, Sonnichsen FD, Sykes BD (1996) The role of transient changes in sample susceptibility in causing apparent multiple-quantum peaks in Hoesy spectra. J Magn Reson Ser A 121:83–87

Malmendal A, Evenas J, Forsen S, Akke M (1999) Structural dynamics in the C-terminal domain of calmodulin at low calcium levels. J Mol Biol 293:883–899

Mock ML, Michon T, van Hest JCM, Tirrell DA (2006) Stereoselective incorporation of an unsaturated isoleucine analogue into a protein expressed in *E. coli*. Chembiochem 7:83–87

Neuhaus D, Williamson MP (2000) The nuclear overhauser effect in structural and conformational analysis. Wiley-VCH Inc, USA

Niccolai N, Spiga O, Bernini A, Scarselli M, Ciutti A, Fiaschi I, Chiellini S, Molinari H, Temussi PA (2003) NMR studies of protein hydration and tempol accessibility. J Mol Biol 332: 437–447

Prosser RS, Luchette PA, Westerman PW (2000) Using O-2 to probe membrane immersion depth by F-19 NMR. Proc Natl Acad Sci USA 97:9967–9971

Prosser RS, Luchette PA, Westerman PW, Rozek A, Hancock REW (2001) Determination of membrane immersion depth with O-2: a high-pressure F-19 NMR study. Biophys J 80:1406–1416

Rinaldi PL (1983) Heteronuclear 2d-noe spectroscopy. J Am Chem Soc 105:5167–5168

Salopek-Sondi B, Vaughan MD, Skeels MC, Honek JF, Luck LA (2003) F-19 NMR studies of the leucine–isoleucine–valine binding protein: evidence that a closed conformation exists in solution. J Biomol Struct Dyn 21:235–246

Strynadka NCJ, James MNG (1989) Crystal-structures of the helix–loop–helix calcium-binding proteins. Annu Rev Biochem 58:951–998

Sykes BD, Weingart HI, Schlesin MJ (1974) Fluorotyrosine alkaline-phosphatase from *Escherichia coli*—preparation, properties, and fluorine-19 nuclear magnetic-resonance spectrum. Proc Natl Acad Sci USA 71:469–473

Teng CL, Hinderliter B, Bryant RG (2006) Oxygen accessibility to ribonuclease a: quantitative interpretation of nuclear spin relaxation induced by a freely diffusing paramagnet. J Phys Chem A 110:580–588

Tjandra N, Kuboniwa H, Ren H, Bax A (1995) Rotational-dynamics of calcium-free calmodulin studied by N-15-NMR relaxation measurements. Eur J Biochem 230:1014–1024

Vaughan MD, Cleve P, Robinson V, Duewel HS, Honek JF (1999) Difluoromethionine as a novel F-19 NMR structural probe for internal amino acid packing in proteins. J Am Chem Soc 121:8475–8478

Wilton DJ, Tunnicliffe RB, Kamatari YO, Akasaka K, Williamson MP (2008) Pressure-induced changes in the solution structure of the Gb1 domain of protein G. Proteins 71:1432–1440

Xiao GY, Parsons JF, Tesh K, Armstrong RN, Gilliland GL (1998) Conformational changes in the crystal structure of rat glutathione transferase M1–1 with global substitution of 3-fluorotyrosine for tyrosine. J Mol Biol 281:323–339

Yu LP, Hajduk PJ, Mack J, Olejniczak ET (2006) Structural studies of Bcl-Xl/ligand complexes using F-19 NMR. J Biomol NMR 34:221–227

Zhang M, Tanaka T, Ikura M (1995) Calcium-induced conformational transition revealed by the solution structure of apo calmodulin. Nat Struct Biol 2:758–767